Defense Technical Information Center
Compilation Part Notice

ADP021461

TITLE: Fast, Feature-Based Wavelet Shrinkage Algorithm for Image Denoising

DISTRIBUTION: Approved for public release, distribution unlimited

This paper is part of the following report:

TITLE: International Conference on Integration of Knowledge Intensive Multi-Agent Systems. KIMAS '03: Modeling, Exploration, and Engineering Held in Cambridge, MA on 30 September-October 4, 2003

To order the complete compilation report, use: ADA441198

The component part is provided here to allow users access to individually authored sections of proceedings, annals, symposia, etc. However, the component should be considered within the context of the overall compilation report and not as a stand-alone technical report.

The following component part numbers comprise the compilation report:
ADP021346 thru ADP021468

Fast, Feature-Based Wavelet Shrinkage Algorithm for Image Denoising

Eric J. Balster and Yuan F. Zheng, Department of Electrical Engineering, The Ohio State University

Columbus, OH 43210 USA, balstere, zheng@ee.eng.ohio-state.edu

Robert L. Ewing, Embedded Information Systems Engineering Branch, Air Force Research Laboratory

Wright-Patterson AFB, OH 45433, robert.ewing@wpafb.af.mil

Abstract—*This paper presents a selective wavelet shrinkage algorithm for digital image denoising. The performance of this method is an improvement upon other methods proposed in the literature and is algorithmically simple for large computational savings. The improved performance and computational speed of the proposed wavelet shrinkage algorithm is presented and experimentally compared with established methods. The denoising methodology incorporated in this new algorithm involves a two-threshold validation process for real-time selection of wavelet coefficients. The two-threshold criteria selects wavelet coefficients based on their absolute value, spatial regularity, and regularity across multiresolutional scales.*

The proposed algorithm takes image features into consideration in the selection process. Statistically, most images have regular features resulting in connected subband coefficients. Therefore, the resulting subbands of wavelet transformed images in large part do not contain isolated coefficients. In the proposed algorithm, after coefficients are selected due to their magnitude, image features in terms of spatial regularity are used to further reduce the number of coefficients kept for image reconstruction.

The proposed wavelet denoising technique is unique in that its performance improved upon several other established wavelet denoising techniques as well as being computationally efficient to facilitate realtime image processing applications.

1. INTRODUCTION

The recent advancement in multimedia technology has promoted an enormous amount of research in the area of image and video processing. Included in the many image and video processing applications such as compression, enhancement, and target recognition are preprocessing functions for noise removal. Noise removal is one of the most common and important processing steps in many image and video systems.

Because of the importance and commonality of preprocessing in most image and video systems, there has been an enormous amount of research dedicated to the subject of noise removal, and many different mathematical tools have been proposed. Variable coefficient linear filters [8, 10], adaptive median filters [3], DCT based solutions [9], cluster filtering [11], etc. have all been proposed in the literature.

The wavelet transform has also been used to suppress noise in digital images. It has been shown the reduction of absolute value in wavelet coefficients is successful in signal restoration [5]. This process is known as wavelet shrinkage. Other, more complex denoising techniques select or reject wavelet coefficients based on their predicted contribution to reconstructed image quality . This process is known as *selective wavelet shrinkage*, and many works have used it as the preferred method of image denoising [2,4–7].

Two of the frontrunners in selective wavelet shrinkage for the removal of noise, Mallat and Hwang prove the successful removal of noise in signals via the wavelet transform, by selecting and rejecting wavelet coefficients based on their Lipschitz exponents [5]. Although this fundamental work in image denoising is successful in the removal of noise, its application is broad and not focused on image noise removal, so the results are not optimal.

Malfait and Roose refined the selective shrinkage denoising approach by applying a Bayesian probabilistic formulation, and modelled the wavelet coefficients as Marcov random sequences [6]. This method is focused on Image de-noising and its results are an improvement upon [5].

Later, Pizurica, et al. continued on the work done by [6]. This work applied a statistical probabilistic model that extended to both spatial and multiresolutional coefficient redundancies to decide on important and unimportant values [7].

Although both algorithms in [6] and [7] give adequate results in denoised image quality, their computational complexities make them impractical for most image and video processing applications.

We have developed a new selective wavelet shrinkage algorithm which has a distinct aspect. It uses a double validation process to select wavelet coefficients for quality image reconstruction. Furthermore, the algorithm is much more efficient in

computational complexity than previous works. The algorithm is comprised of three processing steps which are common to all *selective* wavelet shrinkage algorithms mentioned previously. First, a corrupted image is decomposed into multiresolutional subbands via the wavelet transform. Next, wavelet coefficients are selected or rejected based upon criteria developed by the algorithm designer. Finally, the denoised image is formed by reconstructing the remaining coefficients via the inverse wavelet transform. The processing step of most cost computationally and most important in denoising performance is the coefficient selection process, which calls for effective and efficient criteria to select or reject wavelet coefficients.

This double validation method for selecting wavelet coefficients results in a denoising algorithm which gives improved results upon [5–7], but without the computational complexity. The two-threshold requirement investigates the regularities of wavelet coefficients both spatially and across scales for predictive coefficient selection, providing selective wavelet shrinkage to non-decimated wavelet subbands.

Following the Introduction, Section 2 gives a wavelet overview and theory on the 2D non-decimated wavelet analysis and synthesis filters. The proposed denoising algorithm is applied to non-decimated wavelet coefficients. Section 3 then describes the coefficient selection process prior to selective wavelet shrinkage. Section 4 gives testing results for parameter selection. Section 5 gives the estimation algorithms for proper parameter selection, and Section 6 gives the results and discussion.

2. WAVELET OVERVIEW

Wavelet Filterbank Theory

Let $a_k[n]$ be scaling coefficients of scale k and position n, and let $h[n]$ be the filter coefficients corresponding to the scaling function. From wavelet theory, we know

$$a_{k+1}[n] = \sum_m a_k[m]h[m - 2n], \qquad (1)$$

where the coefficients $a_{k+1}[n]$ represent a coarser resolution then $a_k[n]$. Equation 1 indicates that the scaling function coefficients a_{k+1} scale can be obtained by convolving a reversed $h[n]$ with a_k, and downsampling by two.

Very similarly,

$$d_{k+1}[n] = \sum_m a_k[m]g[m - 2n], \qquad (2)$$

where $d_k[n]$ are the wavelet coefficients of scale k and position n. $g[n]$ is the set of filter coefficients corresponding to the wavelet.

From Equations 1 and 2, we can obtain increasingly coarser scales of scaling coefficients, a_{k+1}, and wavelet coefficients,

$d_{k+1}[n]$, by convolving the scaling function coefficients, $a_k[n]$ by both a reversed scaling function filter, $h[n]$, a reversed wavelet filter, $g[n]$, and downsampling by two. Figure 1 gives a block diagram of the wavelet analysis filterbank.
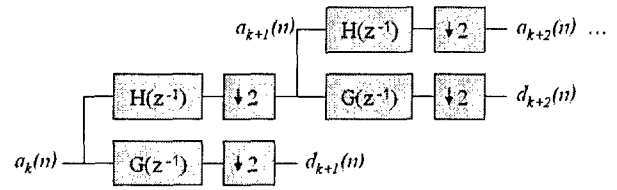

Figure 1 - Wavelet Decomposition

Because each filtered output is downsampled by two, the same number of total coefficients remains the same, regardless of the number of resolution levels, k.

The reconstruction of finer scaling coefficients is obtained by,

$$\begin{aligned} a_k[n] = &\sum_m a_{k+1}[m]h[n - 2m] \\ &+ \sum_m d_{k+1}[m]g[n - 2m]. \end{aligned} \qquad (3)$$

From Equation 3, we can the obtain an arbitrarily fine scale representation of a signal by upsampling the scaling and wavelet coefficients, and filtering the coefficients with their respective filters, $h[n]$ and $g[n]$. The wavelet reconstruction block diagram is given in Figure 2.
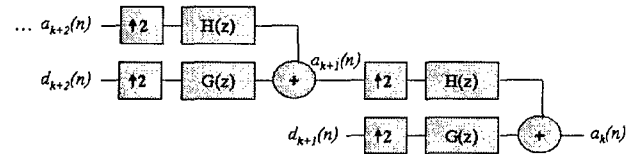

Figure 2 - Wavelet Reconstruction

Non-Decimated Wavelet Transform

In certain applications such as signal denoising, it is not desirable to downsample the wavelet coefficients after decomposition, because the spatial resolution of the coefficients is degraded due to downsampling. Therefore, for the non-decimated case, each subband contains the same number of coefficients as the original signal. So we must have

$$\begin{aligned} \alpha_k[2^{k+1}n] &= a_k[n] \\ \lambda_k[2^{k+1}n] &= d_k[n], \end{aligned} \qquad (4)$$

where $\alpha_k[n]$ are the non-decimated scaling function coefficients, and $\lambda_k[n]$ are the non-decimated wavelet coefficients. We can substitute Equation 4 into Equation 1 to find

$$\begin{aligned} a_{k+1}[n] &= \sum_m h[m]a_k[m - 2n] \\ \alpha_{k+1}[2^{k+2}n] &= \sum_m h[m]\alpha_k[2^{k+1}(m - 2n)] \qquad (5) \\ \alpha_{k+1}[n] &= \sum_m h[m]\alpha_k[2^{k+1}m - n]. \end{aligned}$$

723

The 2^{k+1} scalar introduced into Equation 5 is the equivalent of upsampling $h[n]$ by $k+1$ prior to its convolution with $\alpha_k[n]$. Similarly we substitute Equation 4 into Equation 2 to obtain,

$$\lambda_{k+1}[n] = \sum_m g[m]\alpha_k[2^{k+1}m - n]. \qquad (6)$$

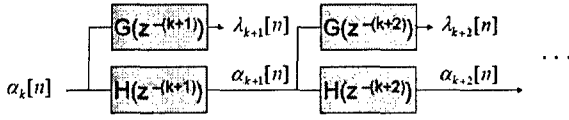Figure 3 gives a block diagram of the non-decimated wavelet decomposition.

Figure 3 - Non-decimated wavelet decomposition

The synthesis of the non-decimated wavelet transform also differs from the downsampled case. From Equation 3, we have

$$a_k[2n] = \sum_m h[2(n-m)]a_{k+1}[m] + \sum_m g[2(n-m)]d_{k+1}[m]. \qquad (7)$$

Substituting $(p = n - m)$ we obtain,

$$a_k[2n] = \sum_p h[2p]a_{k+1}[n - p] + \sum_p g[2p]d_{k+1}[n - p]. \qquad (8)$$

Substituting Equation 4 into Equation 8 we have,

$$\alpha_k[2^{k+2}n] = \sum_p h[2p]\alpha_{k+1}[2^{k+2}(n-p)] \\ + \sum_p g[2p]\lambda_{k+1}[2^{k+2}(n-p)] \quad , \qquad (9)$$

and

$$\alpha_k[n] = \sum_p h[2p]\alpha_{k+1}[n - 2^{k+2}p] \\ + \sum_p g[2p]\lambda_{k+1}[n - 2^{k+2}p]. \qquad (10)$$

Looking at Equation 10 information is being thrown away by downsampling $\alpha_{k+1}[n]$ and $\lambda_{k+1}[n]$ by 2 prior to convolution. Because the downsampling in the analysis filters is eliminated, a downsample by 2 is shown in the synthesis equation, Equation 10. If a downsample by 2 is not performed, i.e. $(m = 2p)$, then we must divide by 2 to provide power equality. That is,

$$\alpha_k[n] = \frac{1}{2}\sum_m h[m]\alpha_{k+1}[n - 2^{k+1}m] \\ + \frac{1}{2}\sum_m g[m]\lambda_{k+1}[n - 2^{k+1}m] \qquad (11)$$

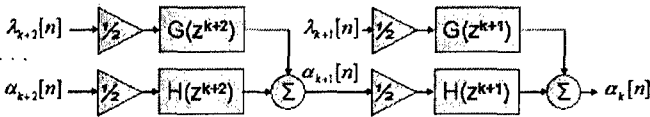Figure 4 gives a block diagram of the non-decimated wavelet transform synthesis.

Figure 4 - Non-decimated wavelet synthesis

We can expand to the two-dimensional case. For a 2-D discrete signal, f we have,

$$\alpha_{ll,k+1}[x,y] = \sum_{n,m} h[n]h[m]\alpha_{ll,k}[2^{k+1}m - x, 2^{k+1}n - y]$$
$$\lambda_{hl,k+1}[x,y] = \sum_{n,m} h[n]g[m]\alpha_{ll,k}[2^{k+1}m - x, 2^{k+1}n - y]$$
$$\lambda_{lh,k+1}[x,y] = \sum_{n,m} g[n]h[m]\alpha_{ll,k}[2^{k+1}m - x, 2^{k+1}n - y]$$
$$\lambda_{hh,k+1}[x,y] = \sum_{n,m} g[n]g[m]\alpha_{ll,k}[2^{k+1}m - x, 2^{k+1}n - y], \qquad (12)$$

where

$$f(x,y) = \alpha_{ll,-1}[x,y]. \qquad (13)$$

The four coefficent sets given in Equation 12 is referred to as the low-low band, $\alpha_{ll,k+1}$, the high-low band, $\lambda_{hl,k+1}$, the low-high band, $\lambda_{lh,k+1}$, and the high-high band, $\lambda_{hh,k+1}$. The sub-bands are named due to the order in which the scaling and/or the wavelet filters process the scaling function coefficients.

For the synthesis of f we have

$$\alpha_{ll,k}[x,y] = \frac{1}{4}\sum_{m,n} h[m]h[n]\alpha_{ll,k+1}[x - 2^{k+1}m, y - 2^{k+1}n] \\ + \frac{1}{4}\sum_{m,n} h[m]g[n]\lambda_{hl,k+1}[x - 2^{k+1}m, y - 2^{k+1}n] \\ + \frac{1}{4}\sum_{m,n} g[m]h[n]\lambda_{lh,k+1}[x - 2^{k+1}m, y - 2^{k+1}n] \\ + \frac{1}{4}\sum_{m,n} g[m]g[n]\lambda_{hh,k+1}[x - 2^{k+1}m, y - 2^{k+1}n] \qquad (14)$$

3. COEFFICIENT SUPPORT

One of the many advantages of the wavelet transform over other mathematical transformations is the retention of spatial information in the wavelet domain. Because of this information retention, there exists a spacial regularity in the sub-bands of wavelet transformed images. Statistically, most images have regular features resulting in connected subband coefficients. Therefore, the resulting subbands of wavelet transformed images in large part do not contain isolated coefficients. This regularity can aid in deciding which coefficients should be selected for reconstruction, and which should be thrown away for maximum reconstructed image quality. The correlation between coefficients in wavelet sub-bands has been discovered by many works, but our method in which this spacial regularity is exploited is unique.

We start with an image signal corrupted with additive noise, i.e.

$$\widetilde{f}(x,y) = f(x,y) + \eta(x,y), \qquad (15)$$

where $f(x,y)$ is the noiseless 2D signal, $\eta(x,y)$ is a random noise function, and $\widetilde{f}(x,y)$ is the corrupted signal.

The wavelet transform of $\widetilde{f}(x,y)$ generates coefficients, $\widetilde{\lambda}_{.,k}$ using Equations 12 and 13. $\widetilde{\lambda}_{.,k}$ is used to create a boolean coefficient map, $I_{.,k}$.

$$I_{.,k}[x,y] = \begin{cases} 1, |\widetilde{\lambda}_{.,k}[x,y]| > \tau \\ 0, else \end{cases}. \qquad (16)$$

A *valid coefficient* is defined as a coefficient value, $\widetilde{\lambda}_{.,k}[x,y]$, which resuls in $I_{.,k}[x,y] = 1$, hence the coefficient has been selected due to its magnitude.

After coefficients are selected by magnitude, spacial regularity is used to further reduce the number of coefficients kept for image reconstruction.

From $I_{.,k}$ we can count the number of support pixels around a particular $I_{.,k}[x,y]$. $S_{.,k}[x,y]$ is the sum of all $I_{.,k}$ which

support the current boolean value $I_{.,k}[x,y]$; that is, the total number of all *valid coefficient* values which are spatially connected to $I_{.,k}[x,y]$.

We say that a coefficient is spatially connected to another if there exists a path of valid coefficients between the two, in any direction. Figure 5 gives a generic coefficient map. The *valid coefficients* are highlighted in gray. From Figure 5 it can be shown that coefficients A, B, C, and H do not support any other coefficients in the coefficient map. However, coefficients D and F support each other, coefficients E and G support each other, and N and O support each other. Also, coefficients I, J, K, L, M, P, and Q all support one another.
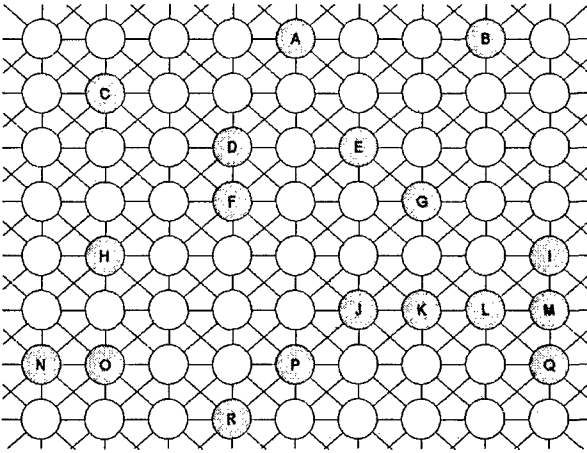

Figure 5 - Generic Coefficient Array

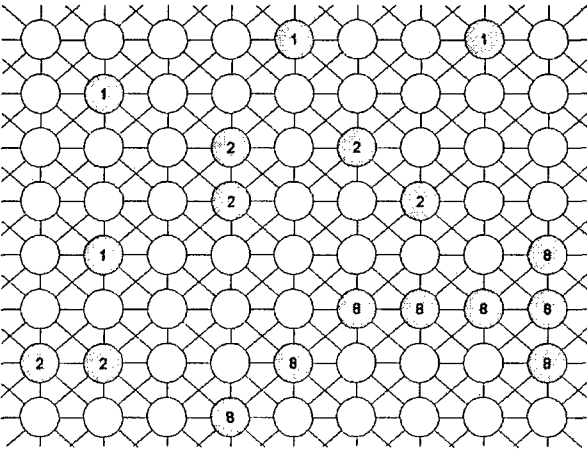Figure 6 gives the value of $S_{.,k}[x,y]$ for each of the *valid coefficients* given in Figure 5.

Figure 6 - Generic Coefficient Array, with corresponding $S_{.,k}$ values

An algorithm for computing $S_{.,k}[x,y]$ is given in the Appendix. $S_{.,k}$ is used to refine the original coefficient map $I_{.,k}$ by

$$J_{.,k}[x,y] = \left\{ \begin{array}{l} 1, S_{.,k}[x,y] > s \\ 0, else \end{array} \right. \quad (17)$$

where $J_{.,k}[x,y]$ is the refined coefficient map, and s is the necessary number of support coefficients.

Not only do coefficients of wavelet transformed images have spatial regularity, they also have regularity across scales. Therefore, to exploit this regularity, we have

$$L_{.,k}[x,y] = \left\{ \begin{array}{l} \widetilde{\lambda}_{.,k}[x,y], J_{.,k}[x,y] + J_{.,k-1}[x,y]I_{.,k}[x,y] > 0 \\ 0, else \end{array} \right.$$
$$(18)$$

The de-noised image is then reconstructed using the supported coefficient values, $L_{,k}[x,y]$ in the synthesis equation given in Equation 14. Thus, we have

$$\begin{array}{l} \hat{\alpha}_{ll,k}[x,y] = \frac{1}{4}\sum_{m,n} h[m]h[n]\hat{\alpha}_{ll,k+1}[x-2^{k+1}m, y-2^{k+1}n] \\ +\frac{1}{4}\sum_{m,n} h[m]g[n]L_{hl,k+1}[x-2^{k+1}m, y-2^{k+1}n] \\ +\frac{1}{4}\sum_{m,n} g[m]h[n]L_{lh,k+1}[x-2^{k+1}m, y-2^{k+1}n] \\ +\frac{1}{4}\sum_{m,n} g[m]g[n]L_{hh,k+1}[x-2^{k+1}m, y-2^{k+1}n] \end{array}$$
$$(19)$$

where

$$\hat{f}(x,y) = \hat{\alpha}_{ll,-1}[x,y]. \quad (20)$$

$\hat{\alpha}_{ll,k}$ and $\hat{f}$ are the reconstructed scaling function coefficients and denoised image, respectively.

4. TEST IMAGES AND SELECTION OF THRESHOLD τ AND SUPPORT s

In the above algorithm, we select wavelet coefficient values based upon a threshold value τ and a support value s. So now we must obtain choices for these values for optimal image denoising. We start with a series of test images, given in Figure 7. These test images are to be used in choosing the values for τ and s.

Figure 7 - Test Images

The test images are all 256x256 in size. Starting from the upperleft image and going clockwise, the images are "Lenna",

725

"Airplane", "Fruits", and "Girl". All of these images are well known standards in the area of image processing.

We begin testing for the optimal values of τ and s by artificially adding Gaussian noise to each of the four images, denoising all four images with a particular τ and s, and recording the average Peak Signal-to-Noise Ratio (PSNR). PSNR of an image is defined by

$$PSNR = 20log_{10}\left(\frac{255}{\sqrt{mse_f}}\right), \qquad (21)$$

where

$$mse_f = \frac{1}{MN}\sum_{x,y}\left(\hat{f}(x,y) - f(x,y)\right)^2. \qquad (22)$$

M and N are the width and height of the images, respectively.

The Haar wavelet is selected for image denoising:

$$h[n] = \begin{cases} \frac{1}{\sqrt{2}} & ,n=0,1 \\ 0 & ,else \end{cases} \quad g[n] = \begin{cases} \frac{-1}{\sqrt{2}} & ,n=0 \\ \frac{1}{\sqrt{2}} & ,n=1 \\ 0 & ,else \end{cases} \qquad (23)$$

The Haar wavelet is used in a non-decimated wavelet decomposition of the original image. 6 subband levels are used, i.e. $k = -1$ to 5. The proposed selective wavelet shrinkage algorithms is applied to all wavelet subbands, and the subbands are synthesized by the non-decimated wavelet inverse transform.

Preliminary tests had shown the Haar wavelet has the most promise in reconstructed image quality. The compact support of the Haar wavelet enables the generation of wavelet coefficients which represent the least amount of original pixel data. Therefore, when a coefficient is removed because of its insignificance. The result affects the least number of pixels in the reconstruction.

We recorded each of the PSNR averages for τ ranging from $0 - 100$ and s ranging from $0 - 15$. We tested the proposed algorithm by applying additive white Gaussian noise (AWGN) with a standard deviation (σ_n) of 10, 20, 30, 40, and 50, to each of the test images. Our method of selective wavelet shrinkage is applied to the corrupted image, and the resulting PSNR is recorded. The results of the testing in which $\sigma_n = 30$ is given in Figure 8.

Figure 9 gives the τ and s which provide the largest average PSNR for each noise level. We will refer to these particular values as τ_m and s_m. Figure 9 suggests that parameters τ_m and s_m are functions of the standard deviation of the artificial noise, σ_n.

5. ESTIMATION OF PARAMETER VALUES

Noise Estimation

It can be shown from the values given in Figure 9 that the parameters τ_m and s_m are functions of σ_n, therefore we can ob-
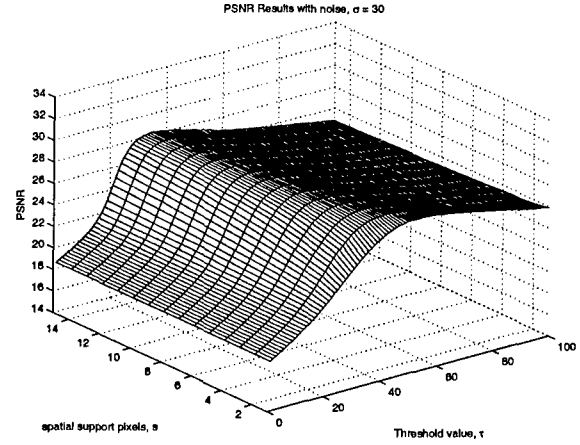

Figure 8 - PSNR Results for Test images, $\sigma_n = 30$

Noise Level (σ_n)	10	20	30	40	50
Max. Avg. PSNR	33.42	30.18	28.34	27.07	26.14
s_m value	2	3	5	9	11
τ_m value	14	28	38	46	62

Figure 9 - Maximum average PSNR of test images for various noise levels and their corresponding threshold and support values

tain an estimate of the optimal values for τ and s from the standard deviation of the noise level. However, the level of noise in a given digital image is unknown. So we must first estimate the noise. Several well known algorithms have been given in the literature to estimate image noise. From [1, 7] a median value of the $\lambda_{hh,0}$ subband is used in the estimation process. However, retrieving the median value in a subband requires a sorting algorithm which is computationally expensive. We propose an averaging noise estimation algorithm. A threshold value, ϵ is used to sort out strong signal (edge) coefficients from the noisy data.

$$\epsilon = \frac{1}{MN}\sum_{x,y}|\lambda_{hh,0}[x,y]|, \qquad (24)$$

where ϵ is a measure of the average magnitude of a coefficient in the $\lambda_{hh,0}$ subband. We also have,

$$\rho[x,y] = \begin{cases} 1, 5\epsilon > |\lambda_{hh,0}[x,y]| \\ 0, else \end{cases} . \qquad (25)$$

In our noise estimation, we use an average of wavelet coefficients instead of a median. The result is a computationally simpler estimate of the image noise. $\rho[x,y]$ is used as a refinement parameter to remove large signal values located in the $\lambda_{hh,0}$ subband. We estimate the noise by,

$$\widetilde{\sigma_n} = \frac{2}{K}\sum_{x,y}\rho[x,y]|\lambda_{hh,0}[x,y]| \qquad (26)$$

where K is the number non-zero terms in the summation of Equation 26.

726

Parameter Estimation

6. RESULTS

Using the known level of noise added to the original images, we can estimate the values of τ_m and s_m given in Figure 9. We use the LMMSE (Linear Minimum Mean Squared Error) as the estimation procedure. That is, we find two parameters a_τ and b_τ such that

$$\widetilde{\tau_m}(\sigma_n) = a_\tau \sigma_n + b_\tau. \tag{27}$$

The choise a_τ and b_τ will minimize the mean squared error (mse):

$$mse_\tau = \sum_{\sigma_n} (\tau_m(\sigma_n) - \widetilde{\tau_m}(\sigma_n))^2. \tag{28}$$

Similarly, we find an estimate of s

$$\widetilde{s_m}(\sigma_n) = a_s \sigma_n + b_s \tag{29}$$

where a_s and b_s are chosen to minimize

$$mse_s = \sum_{\sigma_n} (s_m(\sigma_n) - \widetilde{s_m}(\sigma_n))^2. \tag{30}$$

From the data given in Figure 9, the values of a_τ, b_τ, a_s, and b_s are found

$$\begin{aligned} a_\tau &= 1.14 \\ b_\tau &= 3.40 \\ a_s &= 0.21 \\ b_s &= 0.60 \end{aligned} \tag{31}$$

The values of τ_m and s_m are given in Figure 10 as well as the corresponding LMMSE estimates, given in Equation 31. As given in Figure 10 the estimated values are the best linear fit into the data. Note that the support value $\widetilde{s}$ must be an integer value.
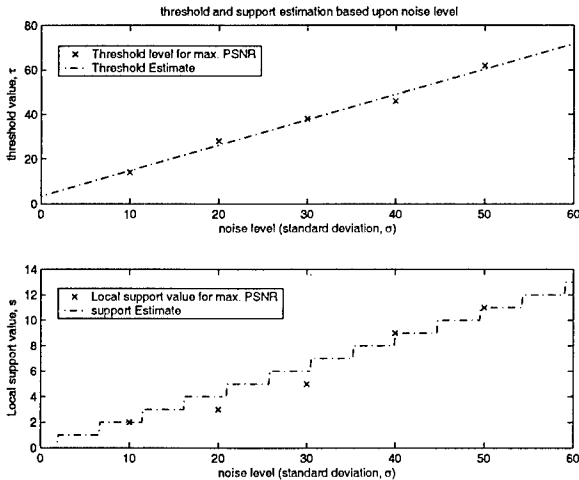

Figure 10 - Optimal values for τ_m and s_m, and their corresponding estimates, $\widetilde{\tau_m}$ and $\widetilde{s_m}$

The threshold value τ and the support value s will be determined by

$$\begin{aligned} \tau &= a_\tau \widetilde{\sigma_n} + b_\tau \\ s &= a_s \widetilde{\sigma_n} + b_s \end{aligned} \tag{32}$$

The images "peppers" and "house" are used for gauging the performance of our denoising algorithm. These two images have also been used in the results of [5–7]. Therefore, we can compare our performace with other recent algorithms given in the literature.

We have corrupted both the peppers image and house image AWGN and used the proposed method for denoising. The results are given in Figures 12 and 13.

Image Input PSNR	"Peppers" 22.6	19.6	16.6	13.6	Average
Proposed Algorithm	30.16	28.63	27.05	25.51	27.84
Pizurica 3-band, [6]	30.20	28.60	27.00	25.20	27.75
Pizurica 2-band, [6]	29.90	28.20	26.60	24.90	27.40
Malfait and Roose, [4]	28.60	27.30	26.00	24.60	26.63
Mallat and Hwang, [5]	28.20	27.30	27.10	24.60	26.80
Matlab's Sp. Ad. Wiener	29.00	27.10	25.30	23.30	26.18

Image Input PSNR	"House" 23.9	20.9	17.9	14.9	Average
Proposed Algorithm	32.50	31.28	30.08	28.85	30.68
Pizurica 3-band, [6]	32.80	31.30	29.80	28.30	30.55
Pizurica 2-band, [6]	32.10	30.50	29.30	28.10	30.00
Malfait and Roose, [4]	32.90	31.30	29.80	28.20	30.55
Mallat and Hwang, [5]	31.30	30.50	29.10	27.10	29.50
Matlab's Sp. Ad. Wiener	30.30	28.60	26.70	24.90	27.63

Figure 11 - PSNR Comparison of the of the proposed method to other methods in the literature
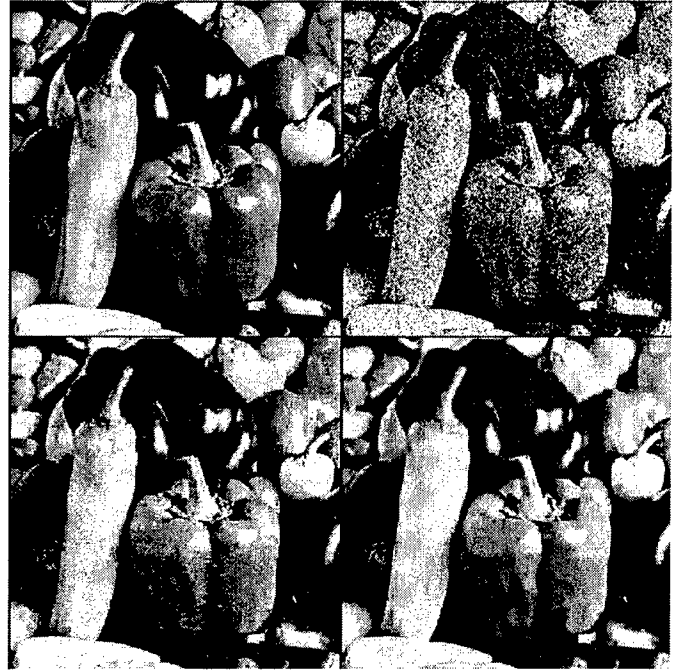

Figure 12 - Results of the proposed image denoising algorithm. Top left: Original "peppers" image, top right: Corrupted Image, $\sigma_n = 37.75$ – PSNR = 16.60, bottom left: denoised image with estimated τ and $s = 0$ – PSNR = 25.76 , bottom right: denoised image with estimated τ and s – PSNR = 27.05

Figure 11 gives the results of our proposed method, as well as the results of [5–7]. As shown in Figure 11, the results of the proposed method are an improvement to other methods described in the literature.

Figure 13 - Results of the proposed image denoising algorithm. Top left: Original "house" image, top right: Corrupted Image, σ_n = 32.47 – PSNR = 17.90, bottom left: denoised image with estimated τ and s = 0 – PSNR = 28.10 , bottom right: denoised image with estimated τ and s – PSNR = 30.08

In addition to improved performance, the proposed algorithm is computationally simple to facilitate real-world applications. However, computational simplicity is a fairly difficult metric to determine when dealing with older literature. The processing ability of modern computers gives more recent literatures' algorithms processing time an unfair advantage. However, the computation time of the proposed method is at least an order of magnitude greater than previous methods, and we have done testing on some older machines for a more accurate comparison. Figure 14 gives the computational results of the proposed method as well as the results of [6,7].

Processor	Pentium IV	Pentium III	IBM RS6000/320H
Proposed Algorithm	2.88	3.70	***
Pizurica 3-band, [6]	***	45.00	***
Pizurica 2-band, [6]	***	30.00	***
Malfait and Roose, [4]	***	***	180.00

Figure 14 - Computation Times for a 256x256 Image, in seconds

Although this is not a true comparison of the difference computational complexity between the proposed algorithm and that of [6,7], the proposed algorithm does show a substantial drop in computation time.

In this paper, a new selective wavelet shrinkage algorithm for image denoising has been described. The proposed algorithm uses a two-threshold support criteria which investigates coefficient magnitude, spatial support, and support across scales in the coefficient selection process. The computationally simple algorithm facilitates real world applications and the performance results are an improvement upon established methods

described in the literature.

7. APPENDIX

The computation of $S_{.,k}[x,y]$ if given from the following algorithm:

$$
\begin{aligned}
&\vec{N}() = \{[-1,-1],[-1,0],[-1,1],[0,-1], \\
&\qquad\qquad [0,1],[1,-1],[1,0],[1,1]\} \\
&O = 0, \ t = 0, \ p = 0, \ \vec{D}_{.,k}(0) = (x,y) \\
&if \ I_{.,k}[x,y] == 1, \\
&\quad while \ \vec{D}_{.,k}(t) \neq NULL, \\
&\qquad (i,j) = \vec{D}_{.,k}(t) \\
&\qquad t = t+1 \\
&\qquad for \ m = 0 \ to \ 7, \\
&\qquad\quad if \ ((I_{.,k}[(i,j) + \vec{N}(m)] == 1) \\
&\qquad\qquad and \ (O[(i,j) + \vec{N}(m)] == 0)), \\
&\qquad\quad p = p+1 \\
&\qquad\quad \vec{D}_{.,k}(p) = ((i,j) + \vec{N}(m)) \\
&\qquad\quad O[(i,j) + \vec{N}(m)] = 1, \\
&\qquad\quad end \ if \\
&\qquad end \ for \\
&\quad end \ while \\
&end \ if \\
&S_{.,k}[x,y] = t
\end{aligned} \tag{33}
$$

$O[x,y]$ is a boolean value to determine whether a particular $I_{.,k}[x,y]$ value has been counted previously. $\vec{D}$ is an array of spatial coordinates of *valid coefficients* that support the current coefficient value $I_{.,k}[x,y]$. $\vec{N}$ is a set of vectors corresponding to neighboring coefficient values.

REFERENCES

[1] D. L. Donoho and I. M. Johnstone. Adapting to unknown smoothness via wavelet shrinkage. *Journal of American Statistical Association*, 90:1200–1224, 1995.

[2] David L. Donoho and Iain M. Johnstone. Ideal spatial adaptation by wavelet shrinkage. *Biometrika*, 81(3):425–455, April 1994.

[3] S. J. Huang. Adaptive Noise Reduction and Image Sharpening for Digital Video Compression.

[4] C. R. Jung and J. Scharcanski. Adaptive Image Denoising in Scale-Space Using the Wavelet Transform. In *XIV Brazilian Symposium on Computer Graphics and Image Processing*, Oct. 2001.

[5] S. Mallat and W. L. Hwang. Singularity Detection and Processing with Wavelets. *IEEE Transcactions on Information Theory*, 38(2):617–623, March 1992.

[6] S. Mallat and W. L. Hwang. Wavelet-Based Image Denoising Using a Markov Random Field A Priori Model. *IEEE Transcactions on Image Processing*, 6(4):549–565, April 1997.

[7] A. Pizurica and M. Acheroy W. Philips, I. Lemahieu. A Joint Inter- and Intrascale Statistical Model for Bayesian Wavelet Based Image Denoising. *IEEE Transcactions on Image Processing*, 11(5):545–557, May 2002.

[8] P. Rieder and G. Scheffler. New Concepts on Denoising and Sharpening of Video Signals. *IEEE Transactions on Consumer Electronics*, 47(3):666–671, August 2001.

[9] M. J. Kim S. D. Kim, S. K. Jang and J. B. Ra. Efficient Block-Based Coding of Noise Images by Combining Pre-Filtering and DCT.

[10] Y. I. Wong. Nonlinear Scale-Space Filtering and Multiresolution System. *IEEE Transactions on Image Processing*, 4(6):774–786, June 1995.

[11] E. Linzer Y. F. Wong, E. Viscito. PreProcessing of Video Signals for MPEG Coding by Clustering Filter. In *International Conference on Image Processing*, volume 2, page 2129, Oct. 1995.